Bulletin of Electrical Engineering and Informatics
Vol. 14, No. 6, December 2025, pp. 4420∼4432
ISSN: 2302-9285, DOI: 10.11591/eei.v14i6.10163

Design and analysis of an asymmetrical star-shaped fractal antenna with meta-surface integration at 5.2 GHz

Piyush Dalsania[1], Jagdish M. Rathod[2]
[1]Electronics and Communication Engineering, Gujarat Technological University, Gujarat, India
[2]Department of Electronics, Birla Vishvakarma Mahavidyalaya, Gujarat, India

Article Info

Article history:

Received Feb 26, 2025
Revised Sep 17, 2025
Accepted Sep 27, 2025

Keywords:

Antenna design
Asymmetrical notch fractal antenna
Radiation efficiency
Return loss
Wireless communication

ABSTRACT

Wireless communication requires optimized antenna designs to ensure maximum signal reception and transmission in today's rapidly advancing technologies. Recent research emphasizes improving antenna efficiency and directivity to support higher data rates, extended coverage, and reliable connectivity. However, conventional antenna structures often suffer from narrow bandwidth, low radiation efficiency, and high return loss, which degrade signal quality and restrict operational range, particularly in complex electromagnetic environments. This study introduces an innovative asymmetrical star-shaped fractal antenna coupled with a metasurface layer consisting of periodic split-ring resonator (SRR) unit cells on a FR4 substrate to overcome these restrictions. The SRR-based metasurface plays a critical role in suppressing surface waves, improving impedance matching, and enhancing radiation directivity. Experimental evaluations were performed across 4.5–10 GHz, focusing on key performance measures such as gain, return loss, and voltage standing wave ratio (VSWR). The suggested antenna achieved a stable return loss below −10 dB and demonstrated a strong operational peak at 5.2 GHz, with improved directivity and radiation efficiency compared to conventional patch designs. The integration of asymmetrical star-shaped fractal geometry with SRR-based metasurface technology effectively addresses the shortcomings of traditional antennas, establishing the proposed design as a compact, efficient, and reliable candidate for mid-band wireless communication systems.

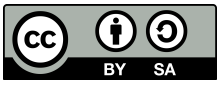

Corresponding Author:

Piyush Dalsania
Electronics and Communication Engineering, Gujarat Technological University
Ahmedabad, Gujarat, India
Email: piyush.dalsania@gmail.com

1. INTRODUCTION

The evolution of wireless technology in recent times has increasingly demanded compact, efficient, and wideband antennas that are easily capable of supporting multiple high data rate applications, requiring both low latency and robust coverage. Mid-band frequencies, such as those used in Wi-Fi (5.2 GHz) and ISM applications, are especially important as they balance coverage and capacity. Antennas for these ranges must achieve superior impedance matching, high gain, and efficient radiation while maintaining a compact footprint suitable for integration in modern wireless devices. In this context, fractal geometries and metasurface structures have gained attention for their ability to enhance antenna performance without significantly increasing size or complexity.

Conventional antenna designs, however, still face challenges in mid-band applications. Traditional microstrip patch antennas, though popular for their simplicity and ease of fabrication, often suffer from narrow bandwidth, low radiation efficiency, and high return loss. These drawbacks restrict operational distance and degrade signal quality, particularly in dense environments where interference is prevalent.

Several improvement techniques such as slotting, defected ground structures (DGS), stacked patches, and dielectric resonators have been proposed. While effective to some extent, they often introduce trade-offs like larger size, fabrication complexity, or limited harmonic suppression. Moreover, few approaches achieve simultaneous improvements in return loss, gain, and efficiency—key requirements for reliable mid-band wireless systems. Similarly, metasurface-enhanced antennas have been widely applied in mmWave and THz bands, but their use in compact mid-band designs for Wi-Fi and ISM systems has not been sufficiently addressed.

To address these issues, this work presents an asymmetrical star-shaped fractal antenna integrated with a metasurface layer on an FR4 substrate. The fractal geometry extends the current path and enhances multi-resonant behavior, while the metasurface, composed of periodic split-ring resonator (SRR) unit cells, suppresses surface waves and improves impedance matching and radiation efficiency. The proposed antenna demonstrates reliable performance with enhanced bandwidth, directivity, and efficiency, making it a compact and effective solution for Wi-Fi and ISM-band mid-band wireless applications.

Recent research has explored fractal and metasurface-based antenna designs with a focus on enhancing bandwidth, polarization control, and radiation performance. These studies can be broadly categorized into four main themes: directivity enhancement, miniaturization and compactness, ground plane effects, and advanced integration approaches.

- Directivity enhancement: several works have aimed at improving antenna directivity and radiation control. Alrashdan *et al.* [1] applied the Taguchi method to optimize patch antenna directivity, demonstrating the effectiveness of systematic optimization. Arenare *et al.* [2] optimized deep-space antennas by combining strut geometry and support structure parameters, while Mejjatti and Habbani [3] proposed innovative designs for high-directivity applications. Okoh and Okhaifoh [4] developed circular microstrip patch antennas with enhanced directivity for base stations, and Galeano and Penagos [5] analyzed mutual impedance in switched-beam arrays to improve directional performance.
- Miniaturization and compact designs: achieving compactness without sacrificing performance has been a key objective. Jahan *et al.* [6] presented compact antenna structures with improved gain, while Sheikh *et al.* [7] introduced a miniaturized Yagi-based antenna tailored for 5G applications. Lu *et al.* [8] explored superdirective microstrip arrays using capacitive loading to push the limits of miniaturization. Jiang *et al.* [9] demonstrated a low-profile tri-port metasurface antenna supporting multiple modes with isolation above 25 dB, showing promise for compact multi-mode operation.
- Fractal and metasurface-based enhancements: fractal geometries and metasurface integration have received particular attention. Yu *et al.* [10] proposed a Koch–Hex fractal antenna achieving bandwidths up to 20.3% across 2.38–5.80 GHz, while Yaminisasi *et al.* [11] designed a Fish-Tail monopole with triple-band resonance for S, C, and X bands. Yadav *et al.* [12] developed a metasurface filtenna with 7.5 dBi gain in the 2.43–2.65 GHz range, though with sharp performance drop outside the band. Barros *et al.* [13] introduced a fractal OAM antenna at 5.88 GHz for circular polarization, while Wang *et al.* [14] proposed a dual-band holographic antenna supporting independent LHCP/RHCP operation. These works highlight the flexibility of fractal and metasurface geometries in achieving wideband and polarization diversity.
- Ground plane effects and environmental considerations: the influence of ground planes has also been studied. Bendaoudi *et al.* [15] investigated graphene ribbon antennas and showed how ground plane modifications affect efficiency and directivity. Singh *et al.* [16] examined return loss and gain-bandwidth trade-offs in defective ground structures as a cost-effective enhancement strategy. Ribeiro *et al.* [17] focused on base station ground antennas for air-to-ground communication links, while Kannadhasan *et al.* [18] studied the environmental effects of 5G radiation, providing insights into societal impacts of antenna deployment.
- Advanced and emerging approaches: finally, recent studies have explored new paradigms. Hao *et al.* [19] presented a metasurface-based channel estimation antenna for handling multipath with a single RF link, albeit with high dependency on tuning. Maeng *et al.* [20] examined 3D antenna radiation effects on UAV communication, while Haque *et al.* [21] integrated machine learning into LTE antenna design, enabling predictive performance optimization. Zhu *et al.* [22] and Prince *et al.* [23] explored beam shaping for satellite communication and direction-finding via Luneburg lenses, respectively, highlighting broader use cases for specialized antenna systems.

– Research gap: while these studies demonstrate significant progress, most focus on either bandwidth enhancement, directivity, or miniaturization individually. Few works simultaneously integrate fractal geometry with metasurface layers to achieve improved impedance matching, radiation efficiency, and stable directivity in compact mid-band antennas suitable for Wi-Fi and ISM applications. This motivates the present work, which introduces an asymmetrical star-shaped fractal antenna with metasurface integration as a unified approach to address these challenges.

2. METHOD

The proposed antenna was designed and optimized in ANSYS HFSS, fabricated on an FR4 substrate, and experimentally validated in an anechoic chamber. The antenna geometry employs an asymmetrical star-shaped fractal structure integrated with a metasurface layer composed of periodic rectangular SRR unit cells. This hybrid configuration was chosen to suppress surface waves, improve impedance matching, and enhance directivity, thereby overcoming the limitations of conventional patch antennas such as narrow bandwidth and high return loss. The combined fractal–metasurface structure minimizes return loss, reduces power reflection, and improves radiation performance at mid-band frequencies. Figure 1 illustrates the triangular fractal ground layer, while Figure 2 presents the complete layered view showing how the radiating patch, dependent notches, feed line, and metasurface are integrated.

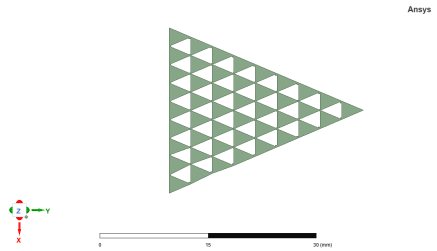

Figure 1. HFSS-simulated triangular fractal ground layer enhancing patch coupling

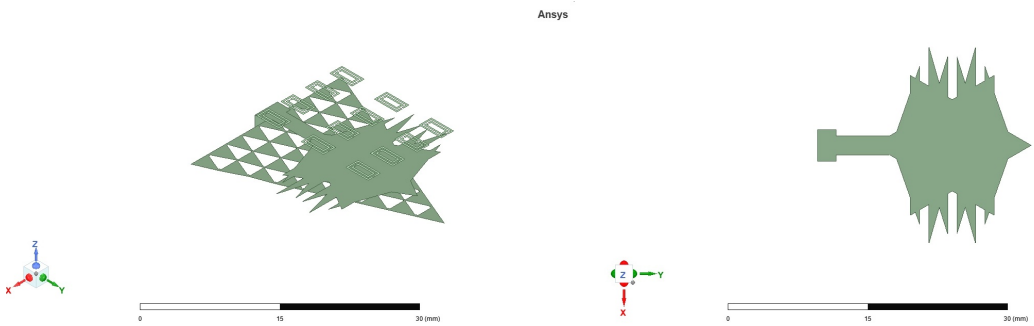

Figure 2. Layered structure of the proposed asymmetrical star-shaped fractal antenna with metasurface and fractal ground

The triangular fractal ground layer (Figure 1) and the asymmetrical star-shaped fractal patch (Figure 2) are integrated in a complementary manner: while the ground fractalization introduces phase discontinuities and improves coupling with the radiating patch, the patch fractalization extends the current path and enhances resonance behavior. This combined effect significantly contributes to the observed improvement in impedance bandwidth, return loss, and radiation efficiency.

2.1. Antenna design specifications

The prototypes are implemented on FR4 substrates and combine an asymmetrical star-shaped fractal geometry with metasurface integration to enhance radiation efficiency, directivity, and impedance matching. The overall antenna structure is shown in Figure 3, while the key design parameters are summarized in Table 1,

covering substrate properties, fractal iteration, notch width, metasurface dimensions, and ground configurations.

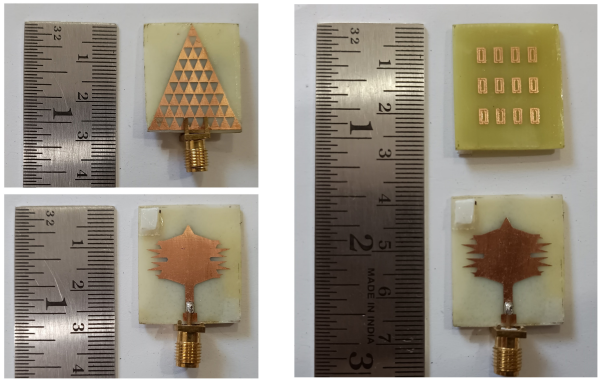

Figure 3. Overview of the proposed asymmetrical star-shaped fractal antenna with metasurface and fractal ground

Table 1. Key design parameters of the proposed asymmetrical star-shaped fractal antenna

Parameter	Value
Substrate material	FR4 ($\varepsilon_r = 4.4$)
Substrate dimensions	32×23×1.6 mm
Fractal iteration level	2 (asymmetrical star-shaped fractal)
Notch width	3 mm
Patch thickness	0.035 mm (copper)
Metasurface unit-cell pitch	4×4 mm
Metasurface layer thickness	0.5 mm
Ground plane configuration	Full/partial (defected ground)

FR4 was selected as the substrate owing to its stable dielectric constant ($\varepsilon_r = 4.4$), robustness, and cost-effectiveness for prototyping. The substrate dimensions of 32×23×1.6 mm^3 and standard copper cladding thickness of 0.035 mm were adopted to maintain compactness while ensuring mechanical durability. The triangular fractal ground plane on the reverse side was incorporated to introduce phase discontinuities, which improved coupling with the radiating patch and enhanced radiation efficiency.

2.1.1. Fractal antenna design

The proposed antenna employs an asymmetrical star-shaped fractal geometry to enhance directivity and support potential multi-band operation. The star-shaped structure introduces multiple arms and edge discontinuities, which effectively increase the current path length and produce additional resonances. This geometry, combined with asymmetrical notches, maintains a compact footprint while enabling improved impedance bandwidth. The fractal arrangement ensures efficient electromagnetic field distribution across the patch, resulting in modified radiation patterns, broadened impedance bandwidth, and improved overall performance.

2.1.2. Notch characteristics

Strategically positioned dependent notches are embedded within the copper patch to control frequency-selective behavior. The notch width ($w_n = 3$ mm) was determined through parametric sweeps in HFSS, where narrower widths reduced coupling efficiency while wider notches increased impedance mismatch. By altering the surface current distribution, the notches extend effective resonant paths and generate additional resonances, thereby broadening the impedance bandwidth. Functionally, the dependent notches act as integrated band-stop filters, suppressing unwanted harmonics while reinforcing desired resonances. This dual role enhances frequency selectivity and contributes to stable performance within the mid-band spectrum.

2.1.3. Metasurface integration

The proposed antenna incorporates a metasurface layer to further optimize radiation behavior and electromagnetic response. The metasurface unit-cell pitch of 4 mm was selected to balance compactness with effec-

tive suppression of surface waves, consistent with prior studies [14]. This choice ensures improved impedance bandwidth and directivity without significantly increasing antenna size. The metasurface modifies the electromagnetic field distribution around the antenna, leading to enhanced directionality and more uniform energy concentration in desired orientations. In addition, it provides fine control of phase and amplitude, supporting applications that demand high polarization purity and directional sensitivity. By shaping current flow and reducing surface-wave losses, the metasurface also improves harmonic suppression and reduces back radiation [24]. Collectively, these characteristics enable the antenna to achieve stable gain, reduced return loss, and efficient operation across the mid-band frequency range.

2.2. Anechoic chamber testing of fractal antenna

The asymmetrical notch fractal antenna was designed and simulated using ANSYS HFSS software to predict radiation behavior, return loss, gain, and directivity under ideal conditions. After fabrication on an FR4 substrate, the prototype was experimentally evaluated in an anechoic chamber to validate the simulations. The chamber provides free-space conditions by absorbing electromagnetic reflections through pyramid-shaped foam absorbers, as illustrated in Figure 4, ensuring accurate measurements without external interference. The testing apparatus utilized a calibrated vector network analyzer (VNA) connected to the antenna via highly reliable, low-loss cables. This minimized the chance of systematic errors. It was mounted on a computer-controlled positioning system that enabled precise azimuth and elevation adjustments for radiation pattern and gain measurements across a wide range of angles. Return loss and voltage standing wave ratio (VSWR) were measured directly from the VNA, while gain and directivity were obtained using a standard gain comparison method with a reference horn antenna. Although the chamber minimizes interference, minor uncertainties remain due to calibration limits, connector losses, and small positioning variations. Based on repeated measurements and equipment specifications, the estimated margins are within ± 0.2 dB for return loss and ± 0.5 dB for gain and directivity, which are negligible compared to the overall performance, confirming the reliability of the results.

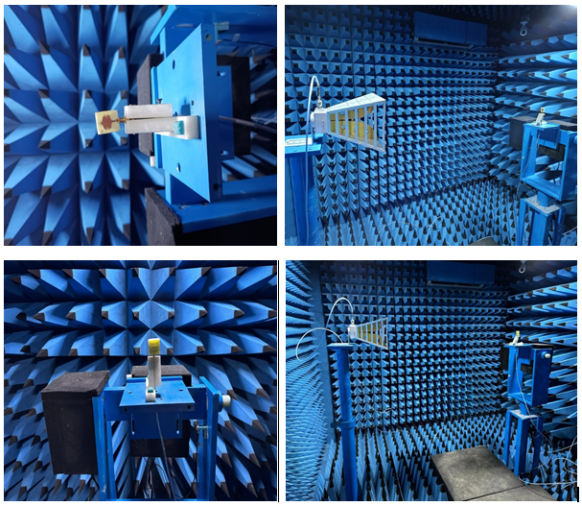

Figure 4. Experimental setup of the fractal antenna inside the anechoic chamber

2.2.1. Ground plane configurations

Three ground plane configurations were modeled in HFSS and fabricated for comparison. In the full ground case, the substrate was backed with a continuous copper layer, serving as the reference. In the partial ground case, the ground plane was truncated to introduce a DGS, modifying surface current distribution and improving impedance matching. In the without metasurface case, the triangular fractal ground was retained but the metasurface layer removed, isolating the effect of the metasurface. These configurations (full, partial, and without metasurface) enabled a systematic evaluation of their impact on return loss, impedance bandwidth, and radiation efficiency.

2.3. Performance optimization

Antenna performance is evaluated using key metrics such as efficiency, return loss, gain, directivity, and VSWR. High efficiency minimizes power losses, while low return loss ensures effective impedance matching and reduced reflections. These parameters are mathematically defined as follows.

Radiation efficiency, denoted as η_r, describes the proportion of input power that is successfully radiated, and is expressed as (1):

$$\eta_r = \left(\frac{P_r}{P_t}\right) \times 100\% \tag{1}$$

where P_r is the radiated power (W) and P_t is the total power delivered to the antenna (W).
The return loss, RL, which quantifies power reflected due to impedance mismatch, is defined as (2):

$$RL = -20\log_{10}\left(|S_{11}|\right) \tag{2}$$

with S_{11} representing the reflection coefficient (unitless).
Antenna gain, G_a, measuring the ability to concentrate energy in a given direction, is given by:

$$G_a = 10\log_{10}\left(\frac{U(\theta,\varphi)}{P_t/4\pi}\right) \tag{3}$$

where $U(\theta,\varphi)$ is the radiation intensity (W/sr) in the direction (θ,φ) and P_t is the transmitted input power (W).
Directivity, D_a, representing the maximum directional concentration of radiated power, is defined as (4):

$$D_a = \frac{4\pi U_{\max}}{P_r} \tag{4}$$

where $U_{\max}$ is the peak radiation intensity (W/sr).
The VSWR, used to evaluate impedance matching, is expressed as (5):

$$VSWR = \frac{1+|\Gamma|}{1-|\Gamma|} \tag{5}$$

where Γ is the reflection coefficient (unitless).

3. RESULTS AND DISCUSSION

3.1. Return loss and bandwidth

The simulated S_{11} response of the proposed antenna across 2.0–7.0 GHz is shown in Figure 5. The antenna exhibited a resonant frequency of 5.2075 GHz with a return loss of -32.67 dB and an impedance bandwidth of 8.5%. These results confirm that the design ensures efficient energy transfer with minimal reflection. The improved impedance matching at this band is directly attributed to the metasurface integration, which suppresses surface waves, and the asymmetrical notch configuration, which extends the current path and stabilizes resonance.

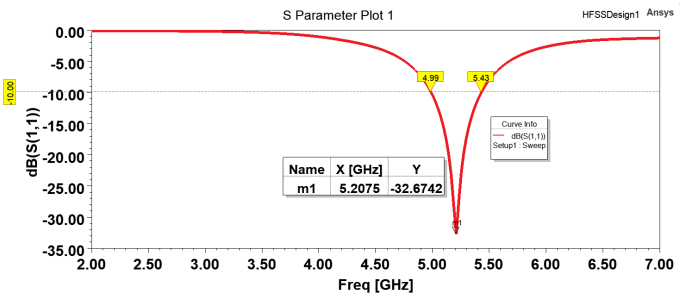

Figure 5. Simulated S-parameter (S_{11}) plot across 2.0–7.0 GHz

The measured reflection loss using VNA is shown in Figure 6, with high and low frequency resonances in Figures 6(a) and (b). The measured resonance also occurs at 5.2075 GHz, with a minimum return loss of –32.67 dB and a measured impedance bandwidth of 440 MHz (4.99–5.43 GHz). These results show close agreement with simulation, with a frequency shift of less than 0.2% and a magnitude difference of only 0.77 dB. The similarity between simulated and measured results demonstrates the effectiveness of the fractal–metasurface configuration in enhancing impedance bandwidth and return loss performance.

(a) (b)

Figure 6. Measured reflection loss (S_{11}) of the fabricated antenna; (a) higher-frequency resonance and (b) lower-frequency resonance

3.2. Voltage standing wave ratio analysis

The VSWR plot, shown in Figure 7, evaluates impedance matching of the antenna across 1.00–9.75 GHz. An ideal VSWR of 1.0 corresponds to perfect matching, with values below 2 generally considered acceptable. The antenna exhibits optimal performance at 5.2075 GHz with a VSWR of 1.0476, approaching the ideal and confirming maximal power absorption with minimal reflection. This strong impedance matching is achieved through the combined influence of the asymmetrical notch fractal geometry, which fine-tunes the surface current distribution, and the metasurface layer, which balances phase and amplitude to stabilize resonance. At frequencies below 4.50 GHz, the VSWR rises sharply (exceeding 100), indicating poor matching and higher reflection losses. Above 5.2075 GHz, the VSWR values remain stable though slightly higher than at resonance, reflecting the antenna's tuning around the mid-band. These observations confirm that the design is optimized for efficient operation at 5.2 GHz while retaining adequate performance across a broader spectrum, making it well suited for Wi-Fi and ISM-band mid-band wireless applications.

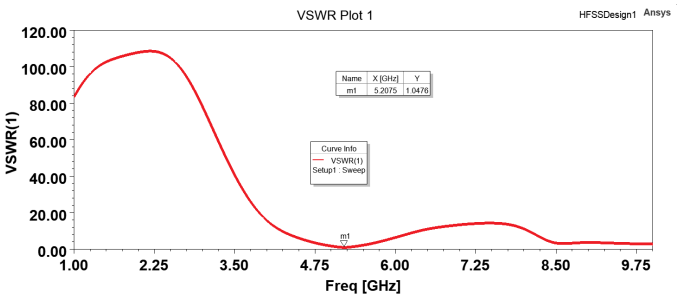

Figure 7. VSWR plot across a wide frequency range for the proposed fractal antenna

3.3. Gain and directivity

The gain and directivity attributes of the antenna, which are important in evaluations, are depicted in Figure 8. This gain plot presents the antenna's capability to capture signals from various directions. It also highlights a peak efficiency of 4.21 dBi and a minimum of -22.62 dBi in certain orientations. The directivity plot demonstrates that the antenna operates as a directional device, attaining a maximum directivity of 5.07 dBi and a minimum of -21.76 dBi relative to isotropic reference levels. These results reveal both strengths and limitations of the antenna. The high maximum values confirm its capability for directional radiation, which is

essential for communication links requiring focused beams, while the negative values simply indicate regions where radiation is significantly weaker compared to isotropic reference. In this context, the negative minimum values represent radiation nulls, which are typical in practical antenna patterns and denote directions of very low or negligible radiated power. Overall, the antenna exhibits strong performance, making it suitable for high-gain directional applications where reduced interference and improved communication quality are critical. The combined assessment of gain and directivity in Figure 8 confirms that this antenna provides reliable point-to-point communication capability.

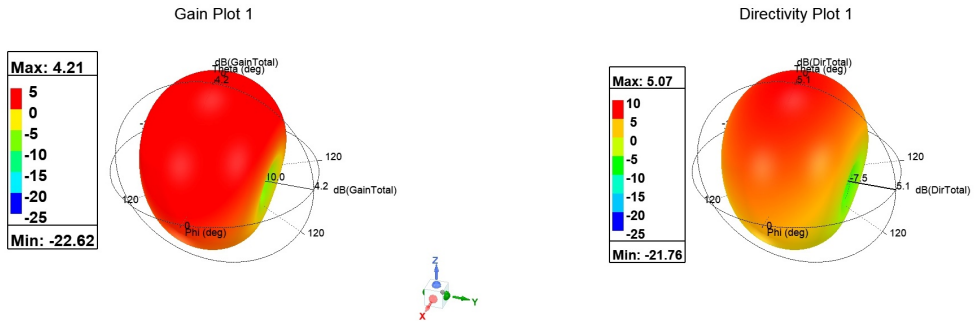

Figure 8. Gain and directivity plots with maximum and minimum values across various angles

3.4. Radiation patterns and axial ratio

The polar radiation characteristics and axial ratio variations of the antenna's array element were compared in three specific orientations, with respect to the plane of the antenna. The results are shown in Figures 9 and 10.

Gain plot 2 (Figure 9(a)) shows radiation levels ranging from -2 dBi to -23 dBi horizontally and from -9 dBi to -16 dBi vertically when oriented at $\Phi = 0°$. The radiation pattern maintains stability across distinct orientations at the same frequency, as seen in gain plot 3 (Figure 9(b)). Circular polarization performance is observed at $\Phi = 0°$ and $\Phi = 90°$, while Figure 10 indicates a notable axial ratio increase at $\Phi = 180°$, suggesting reduced polarization purity. Circular polarization benefits satellite, RFID, and IoT applications by reducing polarization mismatch and improving link reliability. The stable axial ratio confirms suitability for such systems, though optimization is needed at $\Phi = 180°$. Overall, the antenna shows strong potential for mid-band applications requiring polarization diversity and robust performance.

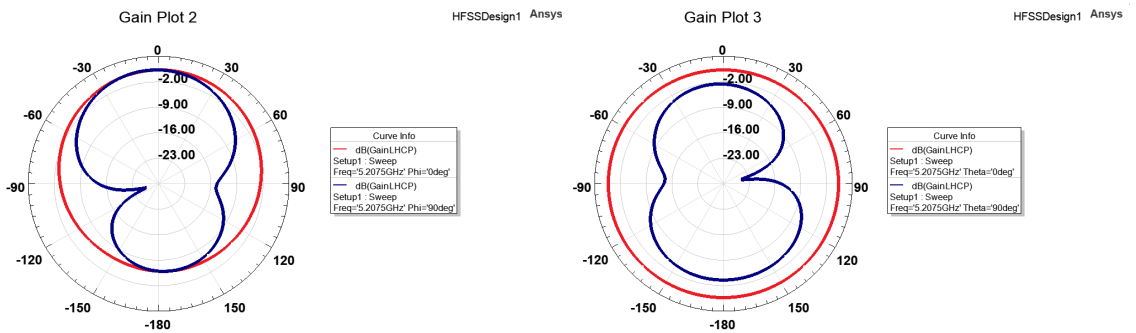

(a) (b)

Figure 9. Polar radiation characteristics of the proposed antenna at $f = 5.2075$ GHz; (a) gain plot 2 for $\Phi = 0°$ and $\Phi = 90°$ and (b) gain plot 3 for $\Theta = 0°$ and $\Theta = 90°$

3.5. S-parameter and impedance

The S-parameter chart, shown in Figure 11, illustrates the reflection characteristics at 5.2075 GHz, specifically examining the S_{11} parameter. The notably low reflection coefficient highlights superior impedance

matching, which is indicative of efficient power transmission, a critical aspect for antennas operating at high frequencies. The chart also details both the resistive and reactive components of the antenna's impedance, confirming its high efficiency in managing high-frequency signals.

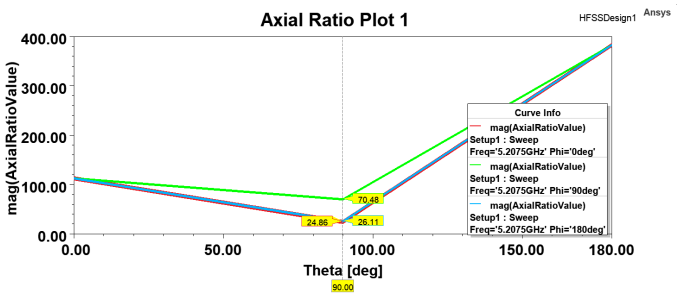

Figure 10. Axial ratio variations at 5.2075 GHz for $\Phi = 0°$, $\Phi = 90°$, and $\Phi = 180°$ orientations

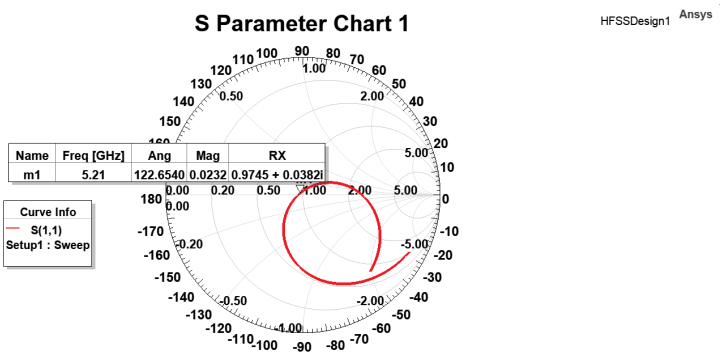

Figure 11. S-parameter chart showing reflection characteristics at 5.2075 GHz

Figure 12 presents a detailed examination of the gain and directivity attributes of the antenna across 5.00–6.00 GHz, with emphasis on 5.2075 GHz. At this frequency, the antenna attains a gain of 4.2132 dBi and a directivity of 5.0692 dBi, demonstrating its ability to amplify signal strength and focus energy effectively compared to an isotropic radiator. The gain curve (green) rises toward 5.2075 GHz, peaks at resonance, and then declines, indicating the antenna's optimal operational bandwidth centered around 5.2075 GHz. Meanwhile, the directivity curve (red) remains relatively stable, peaking slightly at the same frequency. This stability confirms a focused radiation pattern, essential for efficient energy utilization and effective signal transmission. This concludes that the antenna is well equipped for targeted communication and offers exceptional clarity and range, which are necessary for optimal performance.

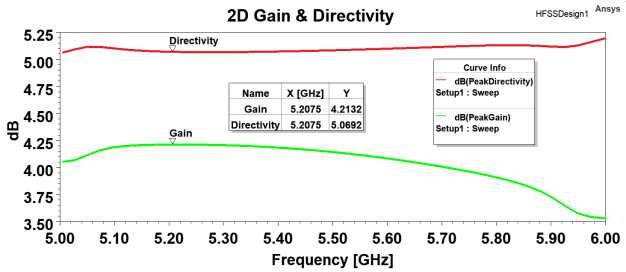

Figure 12. Antenna gain and directivity over the frequency range of 5.00–6.00 GHz

3.6. Efficiency and radiation intensity

Figure 13 presents the radiation efficiency and normalized peak radiation intensity of the antenna between 5.00–6.00 GHz. As shown in Figure 13(a), the radiation efficiency reaches a maximum of 0.8211 (i.e.,

82.11%) at 5.2075 GHz, confirming optimal power conversion at resonance. Similarly, Figure 13(b) illustrates that the normalized radiation intensity peaks at 0.2098 (i.e., 20.98%) at the same frequency, demonstrating the antenna's strong directional transmission capability. These results emphasize the importance of precise frequency tuning to maintain efficiency and polarization integrity in high-performance wireless applications.

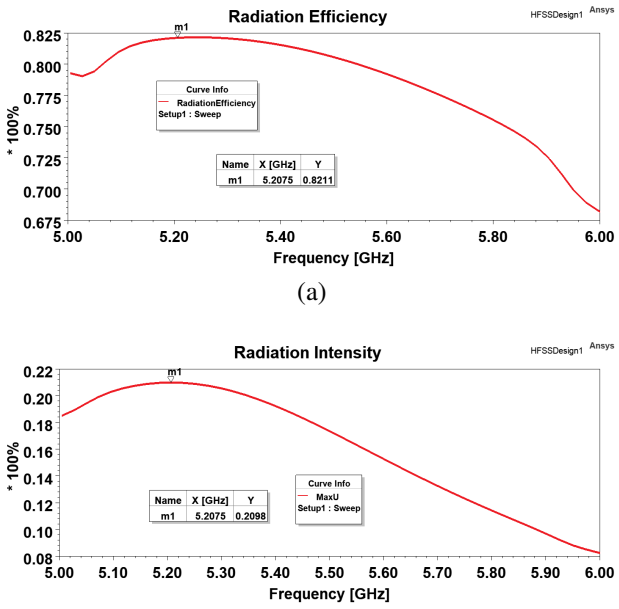

Figure 13. Antenna performance between 5.00–6.00 GHz; (a) radiation efficiency and (b) radiation intensity with peaks at 5.2075 GHz

3.7. Power handling and ground effects

Figure 14 summarizes the antenna's power handling capability and the influence of ground configurations. As shown in Figure 14(a), the accepted power at 5.2075 GHz is 29.9977 dBm, while the radiated power is 29.1417 dBm, corresponding to a small loss of 0.856 dB due to resistive and dielectric inefficiencies. The accepted power remains nearly constant across the studied band, whereas the radiated power shows a slight roll-off at higher frequencies, suggesting potential for further optimization. Figure 14(b) compares the return loss performance for three ground configurations: full ground, partial ground, and without metasurface. The partial ground setup demonstrates superior impedance matching with a return loss of approximately –30 dB at 5.46 GHz, while the full-ground and no-metasurface cases exhibit weaker performance with shifted resonances. These results confirm that ground plane engineering plays a critical role in enhancing antenna efficiency and impedance stability.

3.8. Comparative analysis with recent studies

A comparative examination of the proposed antenna against contemporary designs is provided in Table 2. The table delineates essential metrics such as antenna dimensions, operational bandwidth, peak gain, and radiation efficiency, underscoring the benefits of the asymmetric star-shaped fractal design with metasurface integration. The proposed design features a compact footprint of 32×23×1.6 mm^3, achieving a bandwidth of 8.5% (4.99–5.43 GHz), a peak gain of 4.21 dBi at 5.2075 GHz, and radiation efficiency of 82.11%. The diagonal square fractal (DSF) antenna [24] (20.42×22.71×4.72 mm^3) achieves higher efficiency (93.34–96%) and peak gains of 2.43 dBi and 7.88 dBi across dual bands, but at the cost of a thicker profile (4.72 mm). The RIS-patch antenna for Wi-Fi [25], with dimensions 60×60×3.6 mm^3, provides a wide bandwidth of 26% (4.98–6.48 GHz) and a peak gain of 6.5 dBi, though its large size limits suitability for compact devices. The reconfigurable varactor-based metasurface antenna [26] offers tunability between 2.6 GHz and 3.4 GHz, with a compact profile of $\sim 0.51\lambda \times 0.49\lambda \times 0.013\lambda$ at 2.6 GHz, achieving 7.5 dBi peak gain and 72–82% efficiency. While its tunability is advantageous, its efficiency is comparable to the proposed design and it targets a different frequency band.

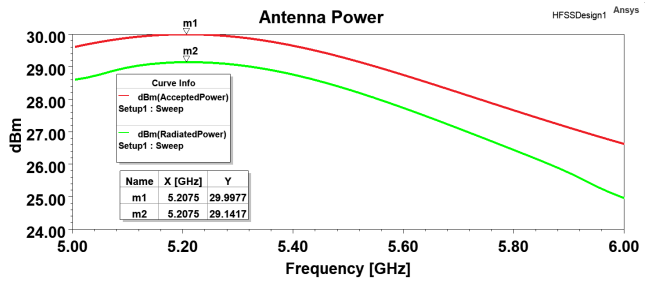

(a)

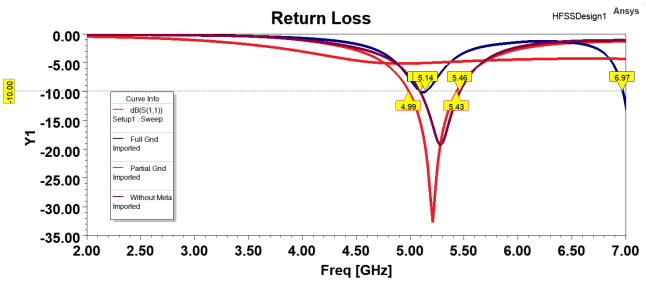

(b)

Figure 14. Antenna performance; (a) power handling and (b) return loss for different ground configurations

Overall, Table 2 demonstrates that the proposed star-shaped fractal antenna provides a balanced trade-off between compact size, stable gain, and high efficiency. Although some existing designs achieve higher bandwidth or tunability, the proposed antenna is designed to perform well in mid-band applications, with a compact structure that provides reliable wireless communication and radar capabilities.

Table 2. Comparison of the proposed antenna with recent state-of-the-art designs

Study	Size (mm^3)	Bandwidth (%)	Peak gain (dBi)	Efficiency (%)
DSF [24]	20.42×22.71×4.72	12.95 @ 5.9, 10.89 @ 9.5 GHz	2.43/7.88	93.34/96
RIS-patch [25]	60×60×3.6	26 (4.98–6.48 GHz)	6.5	–
Varactor [26]	$\sim 0.51\lambda \times 0.49\lambda \times 0.013\lambda$	5 (2.51–2.64 GHz), tunable to 3.4 GHz	7.5	72–82
Proposed	32×23×1.6	8.5 (4.99–5.43 GHz)	4.21 @ 5.2075	82.11

4. CONCLUSION

The design and evaluation of the star-shaped fractal antenna integrated with a metasurface demonstrated robust performance for mid-band wireless communication applications. The antenna achieved a resonance at 5.2075 GHz with a return loss of -32.67 dB and an impedance bandwidth of 8.5% (4.99–5.43 GHz), ensuring effective power transfer with minimal reflection. The VSWR was optimized to 1.0476 at resonance, confirming near-ideal impedance matching. Radiation characteristics showed a peak gain of 4.21 dBi and directivity of 5.07 dBi, validating its capability for directional communication. Furthermore, the radiation efficiency reached 82.11%, while normalized radiation intensity peaked at 20.98% at the same frequency, highlighting strong directional transmission. Power handling analysis indicated an accepted power of 29.99 dBm and radiated power of 29.14 dBm, with only 0.856 dB loss. Ground configuration studies confirmed that partial ground offered superior impedance matching with -30 dB return loss at 5.46 GHz. While the proposed antenna achieves compact size, stable gain, and high efficiency, the study is limited to FR4 substrates and controlled anechoic chamber testing. A key limitation is the relatively narrow bandwidth trade-off and increased fabrication complexity due to fractal and metasurface integration. Future work will focus on evaluating alternative substrate materials for improved bandwidth, validating performance in real-world multipath environments, and extending the design toward true multi-band operation. These directions will further enhance the practicality and versatility of the proposed antenna for next-generation wireless systems.

ACKNOWLEDGMENTS

The research and measurements were carried out at the ELARC – Electromagnetics and Antenna Research Centre, B V M Engineering College, Vallabh Vidyanagar, India, under a contractual arrangement. This research did not receive any specific grant from funding agencies.

FUNDING INFORMATION

No funding was received to conduct this research.

AUTHOR CONTRIBUTIONS STATEMENT

This journal uses the Contributor Roles Taxonomy (CRediT) to recognize individual author contributions, reduce authorship disputes, and facilitate collaboration.

Name of Author	C	M	So	Va	Fo	I	R	D	O	E	Vi	Su	P	Fu
Piyush Dalsania	✓	✓	✓	✓	✓	✓	✓	✓	✓	✓			✓	
Jagdish M. Rathod		✓				✓		✓	✓	✓	✓	✓		

C : **C**onceptualization
M : **M**ethodology
So : **So**ftware
Va : **Va**lidation
Fo : **Fo**rmal Analysis
I : **I**nvestigation
R : **R**esources
D : **D**ata Curation
O : Writing - **O**riginal Draft
E : Writing - Review & **E**diting
Vi : **Vi**sualization
Su : **Su**pervision
P : **P**roject Administration
Fu : **Fu**nding Acquisition

CONFLICT OF INTEREST STATEMENT

The authors declare that there are no conflicts of interest regarding the publication of this paper.

DATA AVAILABILITY

Derived data supporting the findings of this study are available from the corresponding author [initials: PD] on request.

REFERENCES

[1] M. H. S. Alrashdan, Z. Al-qudah, and M. Al Bataineh, "Microstrip patch antenna directivity optimization via Taguchi method," *Ain Shams Engineering Journal*, vol. 15, no. 9, pp. 1-13, 2024, doi: 10.1016/j.asej.2024.102923.

[2] D. Arenare, F. Pelorossi, F. Concaro, and M. Pasian, "On the effects of struts diameter and shape on the European Space Agency deep space antenna directivity and first side lobe," *International Journal of Microwave and Wireless Technologies*, vol. 16, pp. 852-861, 2024, doi: 10.1017/S1759078724000527.

[3] M. El Mejjatti and A. Habbani, "Innovative model for predicting soil impact on patch antenna directivity," in *2023 6th International Conference on Advanced Communication Technologies and Networking (CommNet)*, Rabat, Morocco, 2023, pp. 1-6, doi: 10.1109/CommNet60167.2023.10365308.

[4] S. Okoh and J. E. Okhaifoh, "Design of a Circular Micro-strip Patch Antenna for Improved Directivity and Gain of Mobile Communication Base Station," *Journal of Engineering Research and Reports*, vol. 26, no. 5, pp. 220–236, 2024, doi: 10.9734/jerr/2024/v26i51149.

[5] L. F. R. Galeano and H. P. Penagos, "Effect of size on mutual impedance coupling in a smart switched-beam antenna array," *Ciencia, Ingenierías y Aplicaciones*, vol. 6, no. 2, pp. 81–104, 2023, doi: 10.22206/cyap.2023.v6i2.2987.

[6] N. A. Jahan, Z. Zafar, and Md. A. Hossain, "Design, Fabrication and Performance Analysis of a Compact Unidirectional Quasi-Yagi Antenna for High Gain and High Directivity at 6.2 GHz," *International Journal of Electrical and Electronics Research*, vol. 12, no. 2, pp. 581–589, 2024, doi: 10.37391/IJEER-120233.

[7] J. A. Sheikh, R. Rehman, Z. A. Bhat, I. S. Masoodi, S. Ashraf, and S. A. Parah, "Miniaturized planar defected ground structure antenna enabled with Yagi directors for enhanced gain performance in mm-wave 5G applications," *Journal of Electromagnetic Waves and Applications*, vol. 38, no. 13, pp. 1419-1434, 2024, doi: 10.1080/09205071.2024.2378051.

[8] P. Lu *et al.*, "Compact Superdirective Microstrip Antenna Array Using Capacitively Loaded Loops on High Dielectric Substrate," *IEEE Antennas and Wireless Propagation Letters*, vol. 23, no. 4, pp. 1351-1355, April 2024, doi: 10.1109/LAWP.2024.3355703.

[9] Z. Jiang, S. Meng, L. Nie, J. Qi, and F. Ji, "A Low-Profile Tri-Port Multimode Metasurface-Based Antenna Using Characteristic Mode Analysis," *IEEE Antennas and Wireless Propagation Letters*, vol. 24, no. 5, pp. 1119-1123, May 2025, doi: 10.1109/LAWP.2025.3527036.

[10] Z. Yu *et al.*, "A New Koch and Hexagonal Fractal Combined Circular Structure Antenna for 4G/5G/WLAN Applications," *Electronics*, vol. 14, no. 2, pp. 1-19. 25, doi: 10.3390/electronics14020237.

[11] G. Yaminisasi *et al.*, "Fish-Tail Structured Fractal Monopole Printed Antenna with Dual Broadband Characteristics for Sub–6GHz 5G and X–Band Radar Applications," *Fractal and Fractional*, vol. 9, no. 1, pp. 1-19, 2025, doi: 10.3390/fractalfract9010029.
[12] A. S. Yadav, S. Sharma, D. Sigroha, and A. Sharma, "Metasurface Equipped Circularly Polarized Two-Port Filtering Dielectric Resonator Antenna for 2.5/2.6 GHz Band," *International Journal of Communication Systems*, vol. 38, no. 3, 2025, doi: 10.1002/dac.6122.
[13] T. A. C. Barros, G. Fontgalland, F. L. Teixeira, P. H. F. Silva, and E. E. C. Oliveira, "Low-Profile Circular-Polarized Fractal Antenna Design With Reduced Orbital Angular Momentum Beam Divergence," *Electronics Letters*, vol. 61, no. 1, 2025, doi: 10.1049/ell2.13192.
[14] P. Wang, G. Xu, B. Yin, and W. Wang, "Dual-Band Dual-Circularly Polarized Tensor Holographic Metasurface Antenna for IoV Sensing and Communications," *IEEE Internet of Things Journal*, vol. 12, no. 10, pp. 14447-14455, 2025, doi: 10.1109/jiot.2024.3525176.
[15] A. Bendaoudi *et al.*, "Effects of ground plane on a square graphene ribbon patch antenna designed on a high-permittivity substrate with PBG structures," *Research Square Preprint*, 2022, doi: 10.21203/rs.3.rs-2036767/v1.
[16] S. Singh *et al.*, "Improvement in Depth–of–Return-Loss & Augmentation of Gain-bandwidth with Defected Ground Structure For Low Cost Single Element mm–Wave Antenna," *International Journal of Computing and Digital Systems*, vol. 16, no. 1, pp. 101–113, 2024, doi: 10.12785/ijcds/160108.
[17] L. N. Ribeiro, S. Hastürkoğlu, and J. Grävendieck, "Ground Base Station Antenna Design for Air-to-Ground Communications," in *2024 18th European Conference on Antennas and Propagation (EuCAP)*, 2024, pp. 1–5, doi: 10.23919/EuCAP60739.2024.10501025.
[18] S. Kannadhasan, K. Venusamy, P. L. Reddy, and R. Nagarajan, "Analysis and optimization of antenna technology based on impacts of 5G radiation on human health and environment," in *International Conference on Wireless Technologies, Networks, and Science 2022: ICWTNS2022*, 2023, vol. 2930, no. 1, doi: 10.1063/5.0175191.
[19] Y. Hao, L. Jin, and S. Xiao, "Fine-Grained Multi-Path Channel Estimation and Matched Reception by Single Metasurface Antenna," *IET Communications*, vol. 19, no. 1, Jan. 2025, doi: 10.1049/cmu2.12871.
[20] S. J. Maeng, H. Kwon, O. Ozdemir, and İ. Güvenç, "Impact of 3D antenna radiation pattern in UAV air-to-ground path loss modeling and RSRP-based localization in rural area," *IEEE Open Journal of Antennas and Propagation*, vol. 4, pp. 1029-1043, 2023, doi: 10.1109/OJAP.2023.3322145.
[21] M. A. Haque *et al.*, "Quasi-Yagi antenna design for LTE applications and prediction of gain and directivity using machine learning approaches," *Alexandria Engineering Journal*, vol. 80, pp. 383–396, 2023, doi: 10.1016/j.aej.2023.08.059.
[22] L. Zhu, X. Pi, W. Ma, Z. Xiao, and R. Zhang, "Dynamic Beam Coverage for Satellite Communications Aided by Movable-Antenna Array," *IEEE Transactions on Wireless Communications*, vol. 24, no. 3, pp. 1916–1933, Mar. 2025, doi: 10.1109/TWC.2024.3514353.
[23] T. J. Prince, M. A. Elmansouri, and D. S. Filipovi, "Cylindrical Luneburg lens antenna systems for amplitude-only direction-finding applications," *IEEE Transactions on Antennas and Propagation*, 2023, vol. 71, no. 10, pp. 7924-7932, Oct. 2023, doi: 10.1109/TAP.2023.3306638.
[24] S. Rajpoot, S. Ghosh, and M. V. Swati, "A Low-Profile, Aperture-Coupled, Diagonal Square Fractal Antenna for Dual-Band Vehicular Communication," *International Journal of Communication Systems*, vol. 38, no. 1, Jan. 2025, doi: 10.1002/dac.70003.
[25] S. K. Budarapu and M. S. Sunder, "A Wide Band Circularly Polarized Antenna Using Meta Surface for Wi-Fi Applications," *Physica Scripta*, vol. 100, no. 3, Jan. 2025, doi: 10.1088/1402-4896/adae40.
[26] S. V. Pande, D. Patil, A. Kumar, A. Tyavlovsky, and A. Muthanna, "Design of a Metasurface Loaded with RF Varactor and PIN Diode Integration Dual-Band Reconfigurable Antenna," *Physica Scripta*, vol. 100, no. 2, Jan. 2025, doi: 10.1088/1402-4896/adac15.

BIOGRAPHIES OF AUTHORS

Piyush Dalsania has received a Bachelor of Engineering in Electronics and Communication Engineering in 2007 from Gujarat University, Ahmedabad. He completed postgraduate studies in communication systems in 2012 at Charotar University of Science and Technology, Gujarat. He is a Ph.D. research scholar in electronics and communication engineering at Gujarat Technological University, Ahmedabad, Gujarat, India. He has filed three patents, authored two international journal papers, presented four international conference papers, and published one book on antenna wave propagation based on his research. He has 15 years of teaching experience in Electronics and Communication Engineering. He can be contacted at email: piyush.dalsania@gmail.com.

Jagdish M. Rathod has received his Bachelor of Engineering and Master of Engineering in Electronics and Communication. He completed his Ph.D. in Microwave and Antenna Engineering in 2011. He has served as a Professor at B V M Engineering College since 1997. He is a Life Member of IETE (India), ISTE (India), IACSIT (Singapore), BES (India), and IAENG (Hong Kong). He has published over one hundred technical and fundamental research papers in international journals and conferences. He has organized more than 40 events, such as seminars, national and international conferences, expert talks, and workshops. He has received a research grant in wireless communication. He can be contacted at email: jmrathod@bvmengineering.ac.in.